steel research international
www.steel-research.de

Automated Tool-Path Generation for Rapid Manufacturing of Additive Manufacturing Directed Energy Deposition Geometries

Max Biegler, Jiahan Wang, Lukas Kaiser, and Michael Rethmeier*

In additive manufacturing (AM) directed energy deposition (DED), parts are built by welding layers of powder or wire feedstock onto a substrate with applications for steel powders in the fields of forging tools, spare parts, and structural components for various industries. For large and bulky parts, the choice of tool-paths influences the build rate, the mechanical performance, and the distortions in a highly geometry-dependent manner. With weld-path lengths in the range of hundreds of meters, a reliable, automated tool-path generation is essential for the usability of DED processes. This contribution presents automated tool-path generation approaches and discusses the results for arbitrary geometries. So-called "zig-zag" and "contour-parallel" processing strategies are investigated and the tool-paths are automatically formatted into machine-readable g-code for experimental validation to build sample geometries. The results are discussed in regard to volume-fill, microstructure, and porosity in dependence of the path planning according to photographs and metallographic cross-sections.

1. Introduction

As additive manufacturing (AM) directed energy deposition (DED) is a relatively new process, little formalized guidelines exist for build-up of individual parts. The automated tool-path generation is generally documented in the literature for numerical control milling applications[1,2] and can partly be adapted to AM. Major differences regarding process-related requirements in comparison with subtractive processing are often a result of the heat input, material addition, and associated effects during build-up. Apart from material selection (powder or wire[3]), quality,[4] and feed rate as well as laser power, forward speed, and feedstock flow,[5] a constant material deposition, heat management, and choice of infill patterns are crucial to the process.[6] In case of a bulk part, where a large area must be filled with material, the repeated thermal cycles significantly influence the microstructural properties of the material. In the literature, several approaches for DED processing exist. Ding et al.[7] presented a hybrid contour-/zig-zag path-planning approach and evaluated the resulting surface roughness in wire-arc-additive-manufacturing of a single layer. Foroozmehr and Kovacevic[8] showed that different path-planning strategies ranging from zig-zag patterns to spirals lead to different temperature flows and resulting residual stresses. Dwivedi and Kovacevic[9] demonstrated that path planning affects the near-net-shape quality of the printed part and so the economic viability of the process in terms of postprocessing effort. Eisenbarth et al.[10] investigated the influence of the build strategy and postprocess milling on the final-shape accuracy. Heigel et al.[11] showed that the orientation of the path planning has significant influence on the substrate distortion during laser cladding. Yadollahi et al.[12] investigated the influence of heat agglomeration and break times between the layers on the mechanical performance of DED tensile specimen.

Figure 1 shows a standard workflow for DED preprocessing from the computer-aided design model to the path planning on the machine. The aim of this publication is to demonstrate the implementation of two automated path-planning strategies for DED, i.e., zig-zag and contour-parallel approaches for a multilayer build. Subsequently, geometry is built with both strategies and the usability is discussed according to the photographs and cross-sections.

2. Path-Planning Strategies

2.1. Zig-Zag Strategy

The implementation of the zig-zag path-planning strategy is shown in **Figure 2** and follows six steps: 1) 2D area generation

M. Biegler, J. Wang, L. Kaiser, Prof. M. Rethmeier
Joining and Coating Technology
Fraunhofer Institute for Production Systems and Design Technology IPK
Pascalstraße 8-9, 10587 Berlin, Germany
E-mail: max.biegler@ipk.fraunhofer.de

Prof. M. Rethmeier
Institute of Machine Tools and Factory Management
Technische Universität Berlin
Straße des 17. Juni 135, 10623 Berlin, Germany

Prof. M. Rethmeier
Welding Technology
Bundesanstalt für Materialforschung und -prüfung (BAM)
Unter den Eichen 87, 12205 Berlin, Germany

The ORCID identification number(s) for the author(s) of this article can be found under https://doi.org/10.1002/srin.202000017.

© 2020 The Authors. Published by WILEY-VCH Verlag GmbH & Co. KGaA, Weinheim. This is an open access article under the terms of the Creative Commons Attribution License, which permits use, distribution and reproduction in any medium, provided the original work is properly cited.

DOI: 10.1002/srin.202000017

Printed by [Wiley Online Library - 095.090.244.032 - /doi/epdf/10.1002/srin.202000017] at [11/05/2020].

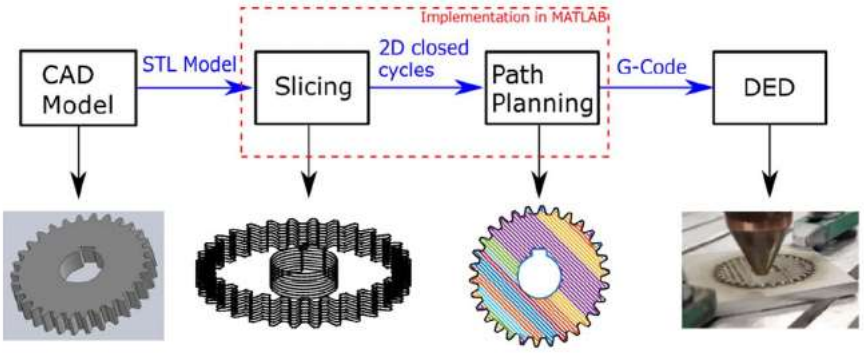

Figure 1. Standard workflow in part setup for the DED process. Slicing, path planning, and translation to the machine have been implemented for this work.

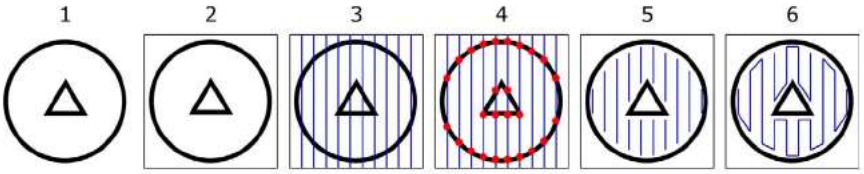

Figure 2. The six steps necessary to generate a tool-path in a sliced 2D geometry.

by slicing the 3D geometry; 2) identification of the smallest bounding box enclosing the 2D area; 3) splitting the bounding box with equidistant lines; 4) finding intersection points between all the lines with the boundary of the 2D area, typically there are multiples of two points per line; 5) trimming the line segments from the points and construction of line segments from these points with offset from the boundary; and 6) connection of ending (or starting) points of each neighbor to form a continuous path.

It is common that more than one continuous path is created during step 6. To prevent the generation of multiple subpaths for one layer, the inclination angle of the equidistant lines in step 3 must be chosen appropriately (**Figure 3**). Single continuous infill paths can be created if the surrounding polygon chain is monotone with respect to a straight line, i.e., the straight lines from point 3 only intersect the sliced geometry twice. If the monotone condition is not met, subpaths are generated, where the process is stopped and continued at the next path's beginning. The beginning and end of the process usually have a higher number of seam irregularities because of start/stop instabilities and should be avoided whenever possible.

2.2. Contour-Parallel Strategy

The contour-parallel pattern displaces outer contours of the sliced geometry inward and inner contours outward in turn. The developed algorithm follows three steps: 1) The 2D boundary contour obtained during slicing is used as an input for this algorithm. Each cycle is either assigned the property internal cycle or external cycle according to their location. An internal cycle is always expanded during offset, whereas an external cycle is shrunk. 2) The path-generation process is initiated and after a contour path is defined. It is offset by a specified distance according to its definition of internal or external cycle. This loop will run until no cycles are created during the offset. After termination,

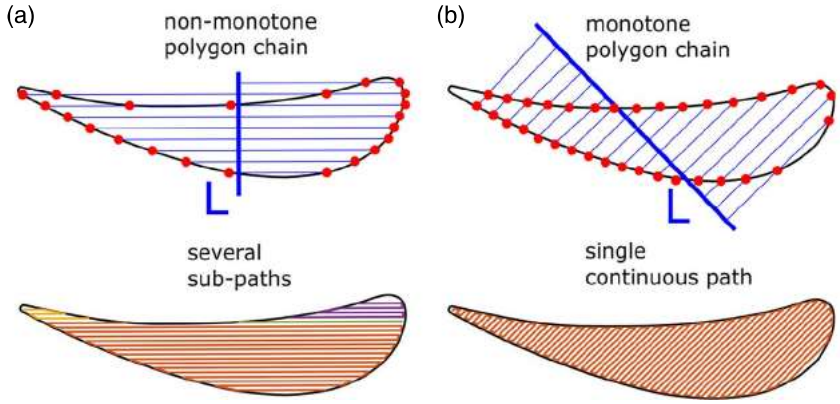

Figure 3. Different choices of inclination angles may result into the generation of subpaths. a) The polygon chain is not monotone with respect to the straight line; therefore, several subpaths are generated. b) The polygon chain is monotone with respect to the straight line; therefore, a continuous path can be created.

© 2020 The Authors. Published by WILEY-VCH Verlag GmbH & Co. KGaA, Weinheim

Printed by [Wiley Online Library - 095.090.244.032 - /doi/epdf/10.1002/srin.202000017] at [11/05/2020].

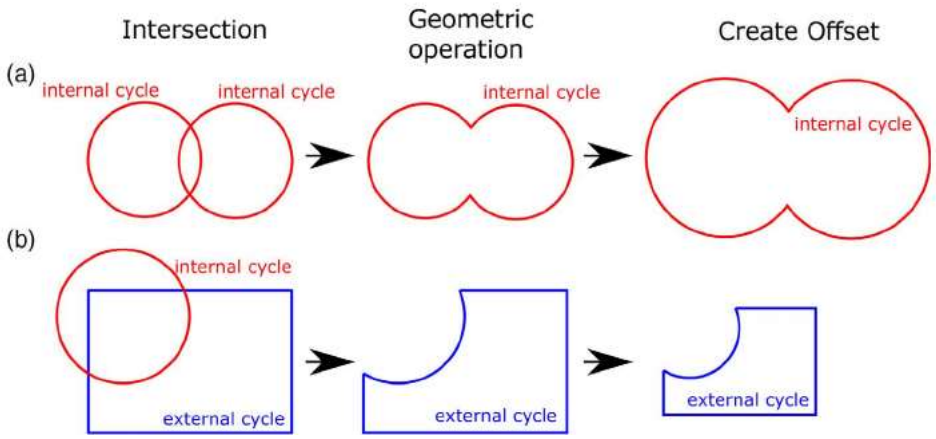

Figure 4. The two special cases encountered while generating contour parallel paths: a) an internal cycle intersection. The cycles are merged, and the resulting cycle is inflated during the offset. b) Intersection between an internal and external cycle: a set difference is created, where the internal cycle is subtracted from the external one. The resulting cycle is assigned the property external cycle and then merged with the current set of cycles (part (b)). The resulting external cycle shrinks during the offset.

the path generation is finished and a matrix contains the trajectories of each tool-path generated in this process. 3) If there are intersections between contours, there are two possible scenarios: a) Intersection between two internal cycles: The union of both intersecting cycles is created and the resulting cycle is assigned the property internal cycle and then merged with the current set of cycles. An example of two intersecting internal cycles creating one new internal cycle is shown in **Figure 4**a. The resulting cycle is inflated during the offset. b) Intersection between an internal and external cycle: A set difference is created, where the internal cycle is subtracted from the external one. The resulting cycle is assigned the property external cycle and then merged with the current set of cycles. Figure 4b shows this scenario. The resulting external cycle shrinks during the offset.

An example of the implemented contour-parallel approach is shown in **Figure 5** for an arbitrary geometry. The initial 2D slice consists of one external cycle (a) and five internal cycles (b)–(f). No intersections occur during the first offset step in (2). During the second offset step, the cycles resulting from (a)–(c) are intersecting. According to the first case in Figure 4, the two internal cycles resulting from (b) and (c) are combined with a new internal cycle. This new cycle is then combined with an external cycle resulting from (a). According to case (b), an external cycle is finally formed and shrunk during (3). For this example, no more cycles are created after six iterations and the path generation is completed.

3. Experimental Section

To validate the path-planning algorithms, a DED component was built using the zig-zag and contour-parallel tool-path generation. The geometry was chosen to be a filled turbine blade cross-section used already in thin-walled form for prior investigations by Biegler et al.[13] and is shown in **Figure 6**.

The experiments were conducted on an EN 1.4404 (AISI 316L) hot-rolled and squared steel substrate with 100 mm side length and 8 mm thickness. The samples were cleaned before the welding process and both sides were rigidly clamped onto the table. A TRUMPF TruLaser Cell 7020 equipped with a 2 kW disc laser and a TRUMPF coaxial powder nozzle to direct the powder flow and argon shielding gas was deployed as cladding system. For all the experiments, AISI 316L (DIN 1.4404) powder feedstock (Metco 41C, grain size 45–106 µm[14]) was used as welding material and 30 s pause time between layers was kept.[15] During the preliminary experiments, bead width was determined to be 1.3 mm for the process parameters shown in **Table 1**, and an offset of 1.0 mm between adjacent lines was chosen to guarantee a good overlap.

In each layer, the processing head first moved along the contour and then filled out the area. This was done four times consecutively with alternating patterns for each strategy. The starting point on the contour for each layer was set to different positions to avoid piling up of deposited material. To compensate for the gradual formation of a downward slope at the edge, an extra layer only consisting of the boundary contour was deposited every four layers. The whole procedure was repeated until the total height of the part reached 12 mm. Subsequently, the part was left to cool until uniform at room temperature and four additional layers were built on top to evaluate the effect of stopping in an ongoing build. The layer-height offset of the zig-zag method amounted to 0.7 mm and the layer offset for the contour-parallel approach was 0.5 mm. The lower achieved height for the contour-parallel method was probably due to lower concentrated heat in the contour-parallel case that led to a decreased powder efficiency.

For the zig-zag strategy, the infill of each manufactured layer alternated between an inclination angle of 45° and 135° in relation to the shown orientation (**Figure 7**) and four different start points to keep process errors from adding up. For each layer, the outer contour was deposited first and, subsequently, the infill pattern was built with 1 mm between adjacent paths. The path planning was repeated every four layers until the desired height was achieved.

The layers of the contour-parallel method alternated between 1 and 0.95 mm offset distance among the infill cycles, so that lines would not be stacked directly on top of one another in the build. This resulted into an outer contour and seven or eight infill cycles each (**Figure 8**). The pattern repeated every four layers with an outside-to-inside direction as well as seven infills for uneven

© 2020 The Authors. Published by WILEY-VCH Verlag GmbH & Co. KGaA, Weinheim

Printed by [Wiley Online Library - 095.090.244.032 - /doi/epdf/10.1002/srin.202000017] at [11/05/2020].

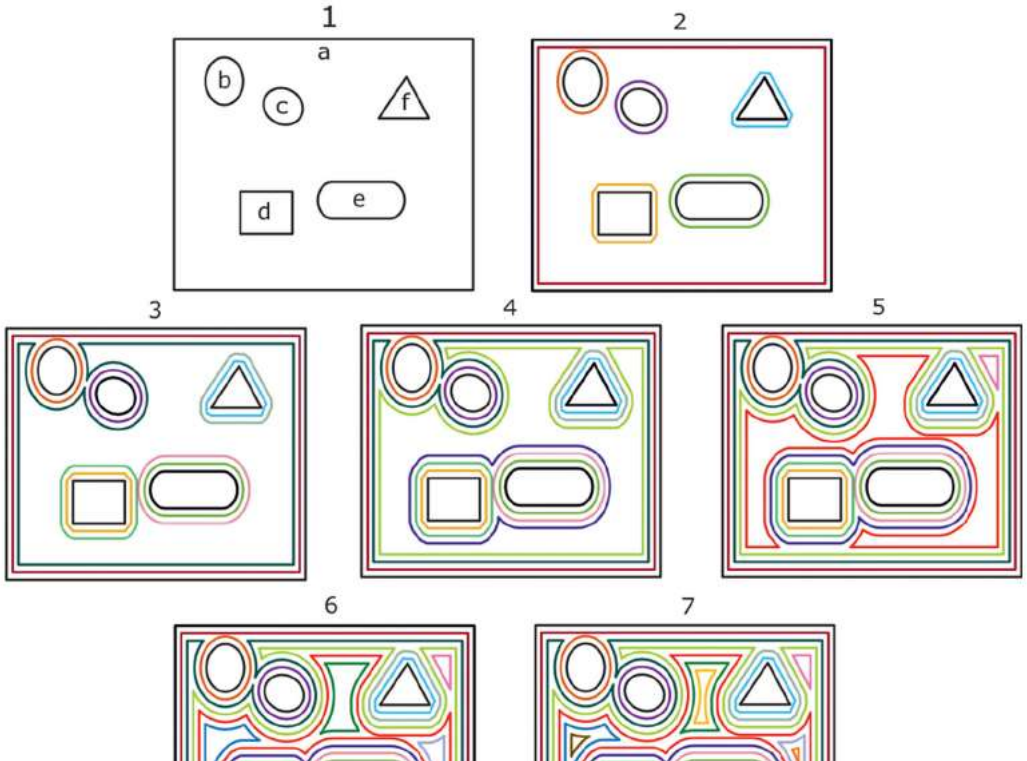

Figure 5. Example of the contour-parallel tool-path generation. The initial geometry consists of one external cycle and five internal cycles. The path generation is finished after six iterations.

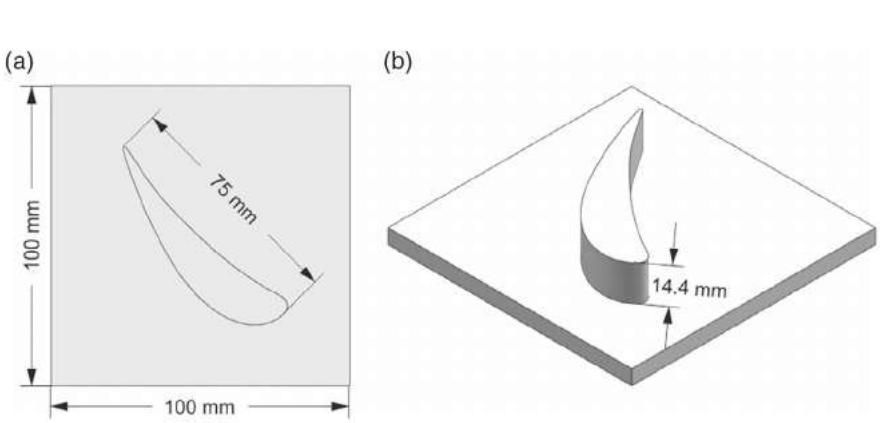

Figure 6. Geometry used for the experimental investigations abstracted from a turbine blade and shown in a) top view and b) side view.

Table 1. Processing parameters.

Laser power [W]	Beam spot diameter [mm]	Forward speed [mm min^{-1}]	Powder flow rate [g min^{-1}]	Pause between layers [s]
600	0.6	600	3.5	30

numbered direction and eight infills for even numbered layers. The start/stop points varied between layers and repeated themselves every four layers. After build-up, one cross-section was prepared for each tool-path strategy and etched using a Bloech und Wedl II solution.[16]

4. Results and Discussion

Figure 9 shows the two resulting parts after build-up to judge the success of the two different path-planning strategies:

© 2020 The Authors. Published by WILEY-VCH Verlag GmbH & Co. KGaA, Weinheim

Printed by [Wiley Online Library - 095.090.244.032 - /doi/epdf/10.1002/srin.202000017] at [11/05/2020].

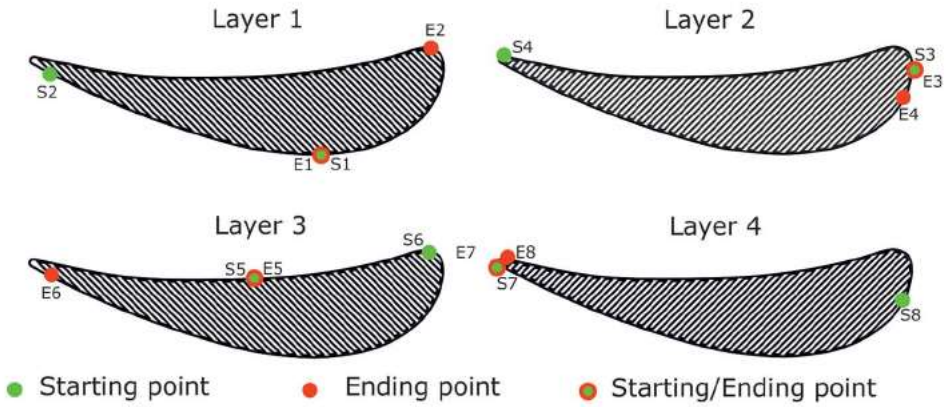

Figure 7. The four different layers in the zig-zag pattern differ by start/stop point of the outer contour as well as for the infill. For layers 1 and 2, the infill direction is from left to right and for layers 3 and 4 it is from right to left.

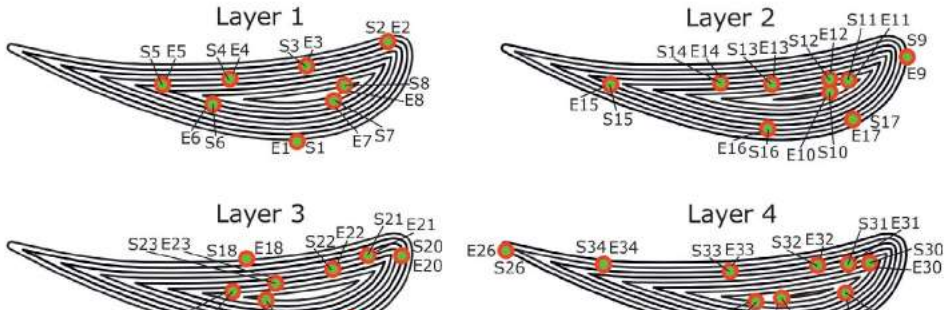

Figure 8. The four different layers in the contour-parallel pattern differ by fill direction and step-over distance. Layer 1 fills from outside to inside with eight contours in total, layer 2 from inside to outside with nine paths. Layers 3 and 4 repeat the cycle but with different start/stop points.

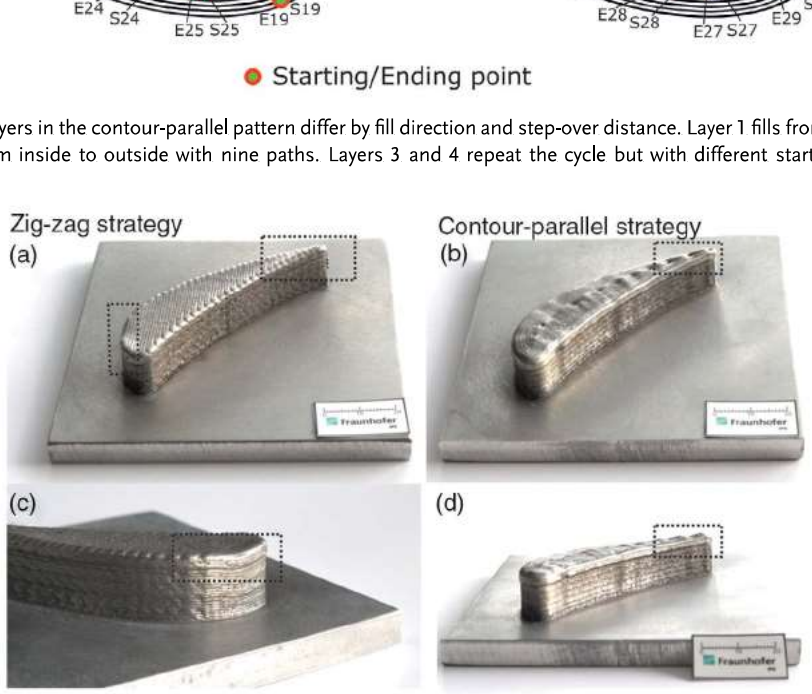

Figure 9. Final parts: a) zig-zag strategy, b) contour-parallel strategy, c) close-up of drop-off in zig–zag strategy, d) side view of the contour-parallel strategy.

Using both strategies, the part can be filled reproducibly. For the zig-zag strategy in Figure 9a,c, the meandering paths connecting the outline are well visible. Two problematic areas are highlighted with dashed boxes. At the rounded side, the

© 2020 The Authors. Published by WILEY-VCH Verlag GmbH & Co. KGaA, Weinheim

Printed by [Wiley Online Library - 095.090.244.032 - /doi/epdf/10.1002/srin.202000017] at [11/05/2020].

geometry is under-filled, dropping at the edge. At the narrow tip, the height rises, eventually moving out of the powder nozzle's focus. The underfill at the round edge constitutes a general problem of straight line-based path planning in so far that radii parallel to the infill direction cannot be filled correctly. Due to the fixed width of a track, it is either underfilled if the last line in the radius is omitted or overfilled if it is added. This is already visible in the path planning shown in Figure 7 (layer 4). Close to point S8, the path cuts off before completely filling the radius. The rising height at the narrow tip is likely due to a heat agglomeration during build-up. As the zig-zag lines get smaller, heat input is concentrated, and the blown powder absorption efficiency rises.

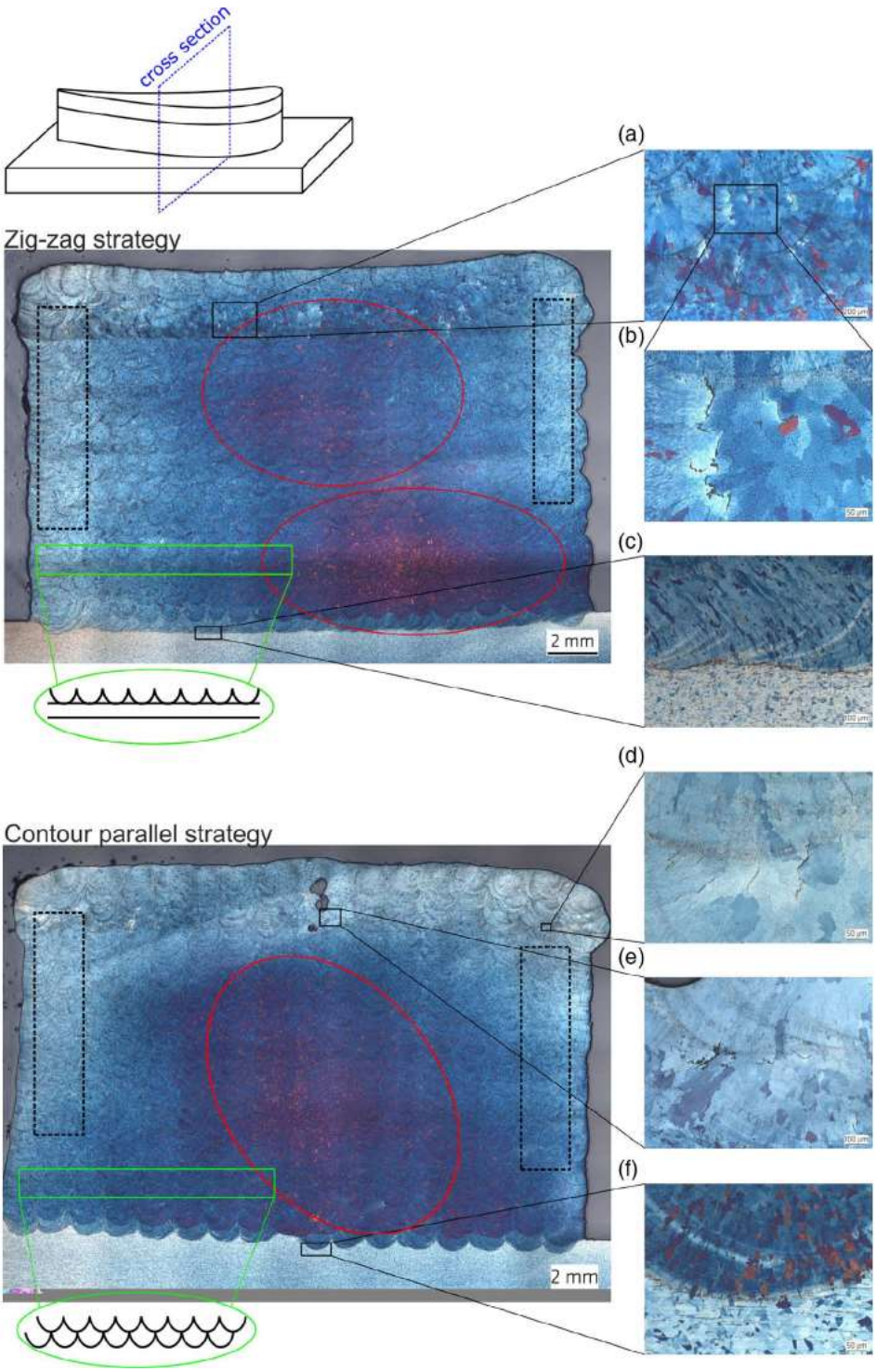

Figure 10. Cross-sections with close-ups for the zig-zag and contour-parallel strategies.

© 2020 The Authors. Published by WILEY-VCH Verlag GmbH & Co. KGaA, Weinheim

Printed by [Wiley Online Library - 095.090.244.032 - /doi/epdf/10.1002/srin.202000017] at [11/05/2020].

This is a problem insofar, as narrow areas rise during a build, requiring readjustment of the DED process or an active process control to reduce laser power when overheating.[17]

For the contour-parallel strategy, (b) is top view showing that the outline is shrunk in consecutive paths to fill the geometry. A good adherence to the contour is visible and no fall-off at the edges occurs. Throughout the part, little pores form, where the pointed areas of the paths meet and in (d) it is visible that the surface is wavy. The pores are likely a result of the path planning itself. Although the contour-parallel strategy can fill rounded areas reliably, it struggles with the sharp angles. Due to the fixed width of a path, angles under a certain critical threshold cannot be filled accurately with consecutive contours and pores remain. At the same time, the machine has to decelerate and accelerate again in the opposite direction, leading to a reduced average forward speed. Without laser-power control, the reduced speed leads to additional material deposition with each layer, causing the wavy surface to form over multiple layers.

To further analyze the result, a metallographic cross-section for one sample of each experiment was manufactured. The cross-sections and close-ups for the direction-parallel and contour-parallel samples are shown in **Figure 10**. In general, a good volume-fill can be observed and the difference in the microstructure of the four top-most layers, where the part was left cool at room temperature before deposition, is well visible.

The top surface of the zig-zag sample is slightly bending downward, whereas material is piling up in the center of the contour-parallel sample. The different planning approaches are visible in the linkage between the manufactured part and the base plate. For the direction-parallel method, the connection line is straight except at the borders. The vaults on both sides indicate the boundary contour, which is deposited prior to the zig-zag infill paths. The linkage between the base plate and the contour-parallel sample (Figure 10c,f) consists of continuous vaults showing that the original boundary contour was shrunk continuously to fill the area. The areas marked by the green border indicate the typical layer structure for each strategy as well. For the direction-parallel approach, a flat layer and a vaulted layer display the alternating inclination angles of 45° and 135°. The different distances between infill cycles of the contour-parallel method are visible as two shifted vaulted layers.

Small cracks are visible throughout the sample (Figure 10b) and especially in the connection to the top four layers added after cooldown. These areas are likely susceptible because of high stress agglomerations in the cooled part that get stressed even during the renewed deposition.

Pores can be found in both samples. They can be caused by absorption of the welding gas in the molten weld pool due to the gas shielding, the laser power, or by quality of the metal powder.[18] In the contour-parallel sample, three large pores can be detected in the center of the top layers. These pores result from the path planning. Especially the last inner cycle generated for layers 1 and 3 reveals that the inner area of the turbine blade can be underfilled if the molten weld material in the upcoming layers is not directed into these gaps and an adjustment of the tool-paths for the top layers is necessary.

The intermixing in the linkage and the typical grain structure of hot rolled steel can be recognized in the close-ups of the substrate (Figure 10c). The 316L metal powder usually forms coarse grains during AM due to the long exposure to elevated temperatures and the directed heat flow in vertical direction.[12] The grain structure on the borders of both samples (area marked with dotted lines) tend to be oriented in height direction because the heat continuously flows downward. In the rest of both samples, no predominant grain orientation can be distinguished.

After etching the cross-sections, the austenitic gamma phase turned blue and red.[16] Both cross-sections show that the austenitic phase is the dominant phase within the built sample, as would be expected from a purely austenitic 316L steel. However, smaller areas of delta ferrite can be observed in the red circled areas, as discussed by Yadollahi et al.[12] The ferritic area of the direction-parallel sample occurs in the center of the upper layers and center-right in the lower layers. For the contour-parallel sample, the area mostly appeared in the center.

5. Conclusion

In this work, an automated approach to generate zig-zag and contour-parallel infill paths for AM DED was shown. The following conclusions are made in this work:

An automated zig-zag pattern generation is described. A continuous infill is dependent on a monotone outline of a given slice and can be adjusted by the inclination angle.

Contour-parallel paths are generated by offsetting the contours inward or outward. Two special cases were considered when contours "collide" while generating the path and the approach was shown for an arbitrary component consisting of outer and inner cycles.

Two filled, turbine blade-shaped parts were built as a proof of concept. At first, photographs were analyzed to identify potential weak points of the path-planning approaches. For the zig-zag strategy, strongly curved and narrow areas were most critical. The contour-parallel pattern had problems with sharp angles, leading to inner cavities and a surface waviness.

The metallographic cross-sections showed a good material fill with elongated, coarse grains common in AM as well as a couple of small cracks and low porosity in the new material. The effect of intermediate cooling at room temperature showed a direct effect in the grain structure.

Overall, it was demonstrated how to adapt tool-path planning approaches from subtractive manufacturing to DED. The performance of different path-planning strategies was shown to be highly geometry dependent, leading to characteristic errors at curved and narrow areas for the zig-zag strategy and at sharp angles for the contour-parallel strategy.

Acknowledgements

The IGF project 18737N of the research association Forschungsvereinigung Stahlanwendung e.V. (FOSTA), Sohnstraße 65, 40237 Düsseldorf, was funded through the AiF within the program of the promotion of the Industrial Joint Research (IGF) by the Federal Ministry for Economic Affairs and Energy based on a resolution of the Deutsche Bundestag.

Printed by [Wiley Online Library - 095.090.244.032 - /doi/epdf/10.1002/srin.202000017] at [11/05/2020].

© 2020 The Authors. Published by WILEY-VCH Verlag GmbH & Co. KGaA, Weinheim

Conflict of Interest

The authors declare no conflict of interest.

Keywords

additive manufacturing, laser metal deposition, mechanical properties, path planning, porosity

Received: January 8, 2020
Revised: April 15, 2020
Published online:

[1] S. Dhanik, P. Xirouchakis, *Int. J. Adv. Manuf. Technol.* **2010**, *50*, 1101.
[2] S. C. Park, B. K. Choi, *Comput. Aid. Des.* **2000**, *32*, 17.
[3] J. C. Heigel, M. F. Gouge, P. Michaleris, T. A. Palmer, *J. Mater. Process. Technol.* **2016**, *231*, 357.
[4] S. Berumen, F. Bechmann, S. Lindner, J.-P. Kruth, T. Craeghs, *Phys. Proc.* **2010**, *5*, 617.
[5] B. Graf, S. Ammer, A. Gumenyuk, M. Rethmeier, *Proc. CIRP* **2013**, *11*, 245.
[6] A. H. Nickel, D. M. Barnett, F. B. Prinz, *Mater. Sci. Eng. A* **2001**, *317*, 59.
[7] D. Ding, Z. Pan, D. Cuiuri, H. Li, *Int. J. Adv. Manuf. Technol.* **2014**, *73*, 173.
[8] E. Foroozmehr, R. Kovacevic, *Int. J. Adv. Manuf. Technol.* **2010**, *51*, 659.
[9] R. Dwivedi, R. Kovacevic, *J. Mech. Eng. Sci.* **2005**, *219*, 695.
[10] D. Eisenbarth, F. Soffel, K. Wegener, *Virtual. Phys. Prototyp.*, **2019**, *14*, 130.
[11] J. C. Heigel, P. Michaleris, T. A. Palmer, *J. Mater. Process. Technol.* **2015**, *220*, 135.
[12] A. Yadollahi, N. Shamsaei, S. M. Thompson, D. W. Seely, *Mater. Sci. Eng. A* **2015**, *644*, 171.
[13] M. Biegler, A. Marko, B. Graf, M. Rethmeier, *Addit. Manufact.* **2018**, *24*, 264.
[14] OC Oerlikon, Material product data sheet austenitic stainless steel powder for thermal spray. https://www.oerlikon.com/oerlikon_DSMTS-0078.5_AusteniticPowders.pdf. (accessed: August 2017).
[15] E. R. Denlinger, J. C. Heigel, P. Michaleris, T. A. Palmer, *J. Mater. Process. Technol.* **2015**, *215*, 123.
[16] E. Weck, E. Leistner, *Metallographische Anleitung zum Farbätzen nach dem Tauchverfahren (Metallographic Instructions for Colour Etching by Immersion)*, Dt. Verl. für Schweisstechnik DVS-Verl., Düsseldorf **1986**.
[17] D. Hu, R. Kovacevic *J. Eng. Manuf.* **2005**, *217*, 441.
[18] M. Khanzadeh, S. Chowdhury, M. A. Tschopp, H. R. Doude, M. Marufuzzaman, L. Bian, *IISE Trans.* **2019**, *51*, 437.

Printed by [Wiley Online Library - 095.090.244.032 - /doi/epdf/10.1002/srin.202000017] at [11/05/2020].

© 2020 The Authors. Published by WILEY-VCH Verlag GmbH & Co. KGaA, Weinheim